

UC Berkeley

UC Berkeley Previously Published Works

Title

Molecular dynamics simulations of internal stress evolution in ultrathin amorphous carbon films subjected to thermal annealing

Permalink

<https://escholarship.org/uc/item/5xq14378>

Authors

Wang, Shengxi
Komvopoulos, Kyriakos

Publication Date

2020-11-01

DOI

10.1016/j.tsf.2020.138247

Peer reviewed



Molecular dynamics simulations of internal stress evolution in ultrathin amorphous carbon films subjected to thermal annealing



Shengxi Wang, Kyriakos Komvopoulos*

Department of Mechanical Engineering, University of California, Berkeley, CA 94720, USA

ARTICLE INFO

Keywords:

Amorphous carbon
Atomic hybridization
Molecular dynamics
Stress analysis
Ultrathin film

ABSTRACT

The evolution of internal stress in ultrathin amorphous carbon (a-C) films is a complex physical process that is difficult to experimentally analyze due to the very small film thickness (a few nanometers) and the lack of instruments that can perform spatiotemporal stress measurements at sub-nanometer resolutions. Even more challenging is the elucidation of the correlation between internal stress, film activation, and temperature. Molecular dynamics (MD) provides potent computational capability for tracking structural changes activated by stress and temperature at the atomic level. Consequently, the aim of this study was to perform a comprehensive MD analysis that elucidates the origin of internal stress in sub-2-nm-thick a-C films grown on single-crystal silicon under optimal deposition energy conditions and explore its dependence on prevalent structural features (e.g., hybridization state) and temperature. The physical mechanisms of a-C film growth and stress built-up under deposition conditions of energetic particle bombardment and stress relief due to thermal annealing are interpreted in the context of MD results. Simulations of film growth illuminate the correlation between film stress and energy of incident carbon atoms. A significant stress relief occurs mainly in the bulk layer of the multilayered a-C film structure at a critical annealing temperature, which continues to intensify with the further increase of temperature. Simulations of time-dependent variation of stress through the film thickness reveal that the stress relief is a very fast process that accelerates with the increase of temperature. The results of this study provide insight into the spatial and temporal variation of internal stress in ultrathin a-C films due to structure and temperature effects and the film stress-structure interdependence.

1. Introduction

The growth of ultrathin amorphous carbon (a-C) films possessing significant fractions of tetrahedral (sp^3) atomic carbon hybridization has been the objective of many studies, mainly because of the well-established correlation between the physical properties and sp^3 content of a-C films. In particular, a-C films with high sp^3 fractions, also known as diamondlike carbon films, have been proven to exhibit high hardness, low friction, excellent chemical inertness, and good thermal stability [1–5]. The combination of these desirable properties has led to the usage of thin a-C films as protective overcoats in a wide range of applications, including automobile and aerospace components, orthopedic implants, optoelectronics, laser lenses, microelectromechanical devices, and hard-disk drives [6–9].

Despite unprecedented industrial applications of a-C films, fundamental studies are still ongoing, principally because establishing correlations between the hybridization state and film stress is challenging for film thicknesses only a few nanometers. Elucidating such correlations is

important because the internal stress can affect the film structure, mechanical integrity, and functionality under various industrial settings [10,11]. According to the generally accepted subplantation theory [12,13], the implantation of energetic particles (film precursors) induces local densification, causing the development of a compressive stress that is conducive to sp^3 hybridization. Because the internal stress depends on the process conditions [14], film growth by techniques encompassing intense particle bombardment, such as ion implantation, reactive sputtering, and filtered cathodic vacuum arc, usually yields a high compressive stress in the film due to localized structural incompatibilities introduced by the impinging energetic particles. However, for a high film stress to be sustained without negatively affecting the adhesive strength at the film/substrate interface, it may be necessary to decrease the film thickness significantly. Several studies have been performed to determine the dependence of internal stress in a-C films on various factors, such as film structure and composition, substrate bias voltage (energy of incident particles), temperature, and post-deposition heat treatment (e.g., thermal annealing) [10,15–19]. Although these studies have provided important

* Corresponding author.

E-mail address: kyriakos@me.berkeley.edu (K. Komvopoulos).

<https://doi.org/10.1016/j.tsf.2020.138247>

Received 1 May 2020; Received in revised form 29 June 2020; Accepted 22 July 2020

Available online 23 July 2020

0040-6090/© 2020 Elsevier B.V. All rights reserved.

guidance for tuning the stress in a-C films by controlling the process conditions, changing the deposition conditions is not always feasible and may alter the film structure and properties. Therefore, a post-deposition heat treatment may be required to relieve the high film stress. Furthermore, in applications involving frictional heating or operation at elevated temperatures, such as high-load bearing components, laser lenses, and heat-assisted magnetic recording devices, changes in film stress may negatively impact the film structure, such as sp^3 to trigonal (sp^2) carbon atom rehybridization.

Traditionally, film stress has been measured by techniques based on the curvature method [14–19]. However, such techniques cannot provide high-resolution, real-time stress measurements, especially for nanometer-thick films undergoing structural changes due to heating. Molecular dynamics (MD) provides an effective alternative for overcoming this experimental scarcity and for obtaining insight into the evolution of stress at atomic and molecular levels. For instance, MD analysis has been used to find the stress field in a metallic substrate indented by a hard ball or a diamond tool [20,21], to explore the generation of dislocations in a Lennard-Jones solid by a penetrating atom [22], to identify the effects of size, shape, and sliding direction of a diamond tip on friction [23], to obtain the subsurface stress field in a face-centered-cubic semi-infinite medium indented by a rigid flat punch [24], and to determine the optimal incident energy range for synthesizing diamondlike carbon films with desirable structures and properties [25]. The foregoing studies have illustrated the potential of MD simulations to elucidate the evolution of structure and internal stress in nanometer-thick films during deposition and heating. Consequently, the objective of this study was to perform a comprehensive MD analysis of the growth and development of internal stress in ultrathin a-C films and to explore the effect of thermal annealing on the film structure and internal stress. The spatiotemporal evolution of the structure and internal stress in a-C films during growth and thermal annealing are examined below in the context of MD simulation results obtained for a wide range of deposition energy and annealing temperature.

2. Molecular dynamics model

The three-dimensional MD model comprises an ultrathin a-C film grown on a $23 \times 23 \times 59.7 \text{ \AA}$ Si(100) substrate consisting of 1620 atoms (Fig. 1). Film growth was simulated for a wide range of deposition energy (i.e., carbon atom kinetic energy) by the sequential deposition of single carbon atoms onto the Si substrate. Fig. 2 shows cross sections of a-C films for deposition energy in the range of 1–120 eV. In each film-growth simulation, 2000 carbon atoms were separately deposited at random positions of the substrate surface at normal incidence. Although the duration of an energetic particle bombardment was only several femtoseconds, the significant energy transferred from the incident carbon atom to the substrate-film system increased the temperature profoundly. To overcome this problem, the silicon substrate atoms were divided into the following three groups. All atoms up to a distance of 13 \AA from the substrate bottom were constrained to simulate a semi-infinite substrate and to fix the substrate position. The atoms in the next 20 \AA were assigned thermostat status, forming a heat bath that equilibrated the system to the nominal temperature of 300 K within 2 ps after each carbon atom impingement. Finally, the remaining atoms at the top region of the model were divided into two subgroups, that is, the atoms inside a cylinder located at the center of the cross-sectional plane of the model were fully unconstrained, whereas the atoms outside this core cylinder were assigned thermostat status and were included in the foregoing heat bath. To simulate film growth on a large substrate, periodic boundary conditions were applied to the lateral faces of the MD model. On the completion of the simulated film growth, a post-deposition relaxation step was used to allow the system to equilibrate at 300 K in 20 ps.

After the simulation of film growth, the a-C film with the highest sp^3 content was subjected to thermal annealing for 50 ns by raising the heat

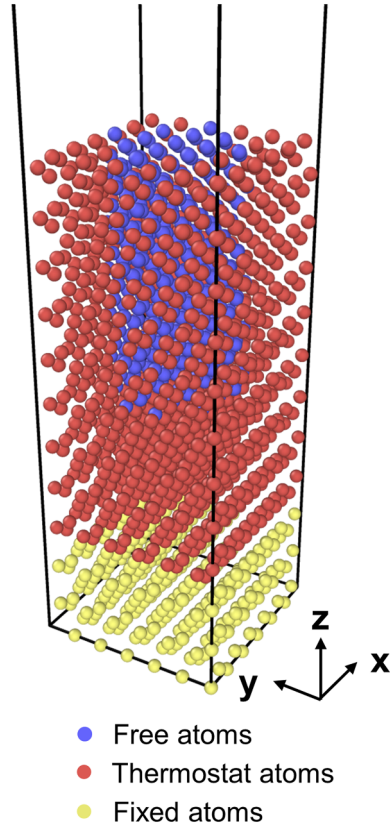


Fig. 1. A perspective view of the Si substrate model. The yellow atoms at the bottom of the model are fixed to simulate a semi-infinite substrate. The red atoms comprise a Berendsen heat bath that is used to control the temperature of the whole model. The blue atoms surrounded by the thermostat atoms are fully unconstrained.

bath temperature. In both film growth and annealing simulations, the damping time assigned to the heat bath was fixed at 100 fs and the time step was set at 0.5 and 0.1 fs, respectively. All the MD simulations were performed with the LAMMPS code.

Atomic interaction in the Si-C system was modelled with the Tersoff interatomic potential E , given by [26,27]

$$E = \sum_i E_i = \frac{1}{2} \sum_{i \neq j} U_{ij} \quad (1)$$

$$U_{ij} = f_C(r_{ij}) [f_R(r_{ij}) + b_{ij}f_A(r_{ij})] \quad (2)$$

where E_i is the potential energy of atom i , U_{ij} is the bonding energy between atoms i and j , r_{ij} is the distance between atoms i and j , f_R and f_A are repulsive and attractive two-body potentials, respectively, and b_{ij} is the so-called bond order that represents the bond strength in the local environment, i.e., the bond strength of atoms with a larger number of neighboring atoms is characterized by a lower potential energy. The Tersoff parametrization detailed elsewhere [26,27] was used to model the Si-C system.

The film stress was calculated as a per-atom-based stress tensor that includes virial and kinetic energy contributions due to interatomic interactions, expressed by [28]

$$\sigma_{ab}^i = -\frac{1}{V^i} \left[\sum_j F_{ij}^a r_{ij}^b + m_i v_i^a v_i^b \right] \quad (3)$$

where σ_{ab}^i are components of the stress tensor of atom i , V^i is the atomic volume assigned to atom i , F_{ij} is the force exerted to atom i by atom j , m_i is the mass of atom i , and v_i is the velocity of atom i . For ultrathin films, the out-of-plane normal stress σ_{zz} is negligibly small compared to the in-

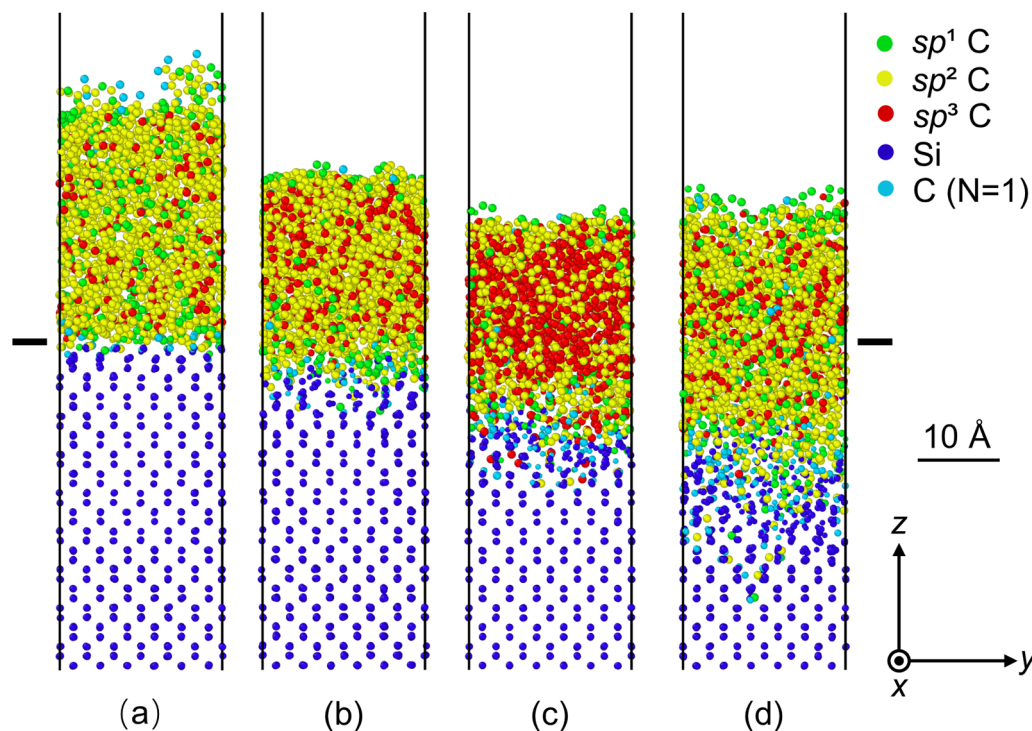


Fig. 2. Simulated a-C film growth on a Si(100) substrate for carbon atom deposition energy equal to (a) 1, (b) 20, (c) 80, and (d) 120 eV. The dark blue circles and the cyan circles represent silicon and carbon atoms with coordination number $N = 1$, respectively. The two black horizontal lines indicate the position of the substrate surface.

plane stresses σ_{xx} and σ_{yy} , which control the internal stress in the film. The magnitude of the hydrostatic (or mean) stress can be associated with the hybridization state. Specifically, a high compressive hydrostatic stress correlates to high sp^3 fraction, whereas a tensile hydrostatic stress favors sp^2 hybridization and may also contribute to film delamination. Thus, the in-plane and hydrostatic stresses not only affect the a-C film structure but may also impact its mechanical integrity. Consequently, these stresses were used in the present analysis to quantify the effects of deposition energy and annealing temperature on the film internal stress. Using Eq. (3), the hydrostatic stress σ_h and the in-plane stress σ_p were computed using the following relations

$$\sigma_h = \frac{\sigma_{xx} + \sigma_{yy} + \sigma_{zz}}{3V} \quad (4)$$

$$\sigma_p = \frac{\sigma_{xx} + \sigma_{yy}}{2V} \quad (5)$$

where V is the volume of a given domain and σ_{kk} ($k = x, y, z$) represents the summation of corresponding tensor components of all the atoms in the particular domain. The hydrostatic and in-plane stresses were calculated by averaging the atomic stresses in 1-Å-thick horizontal slices at various depths from the film surface. The slice volume was computed by multiplying the horizontal cross-sectional area of the model ($23 \text{ \AA} \times 23 \text{ \AA}$) with the slice thickness (1 Å).

3. Results and discussion

The a-C films grown under conditions of deposition energy in the range of 1–120 eV (Fig. 2) demonstrated significant differences in both the morphology and structure (hybridization state). Deposition energy of 1 eV is typical of gas-phase film growth processes, such as evaporation and physical/chemical vapor deposition, whereas deposition energy in the range of 20–120 eV is typical of film growth processes that use energetic particles as film precursors, such as filtered cathodic vacuum arc deposition. The hybridization state can be quantified by the atomic coordination number of an atom, defined as the number of its nearest neighboring atoms. A coordination number equal to 4, 3, and 2 indicates sp^3 , sp^2 , and sp^1 (linear) atom hybridization, respectively. An extremely small number of under-coordinated atoms with coordination

number equal to 1 may also exist at the film surface. Very low deposition energy (1 eV) produced a relatively thick a-C film dominated by sp^2 hybridization [Fig. 2(a)]. Alternatively, a thinner, denser, and significantly rich in sp^3 hybridization a-C film was deposited when the deposition energy was increased to 80 eV [Fig. 2(c)], while the films synthesized under conditions of moderate (20 eV) and high (120 eV) deposition energy, Fig. 2(b) and (d), respectively, demonstrated medium levels of sp^3 hybridization. A comparison of the simulation results shown in Fig. 2 indicates that the a-C film with the highest sp^3 content corresponds to deposition energy of 80 eV. From an analysis of the MD data, the sp^3 content of the a-C films for deposition energy equal to 1, 20, 80, and 120 eV was found equal to 11%, 22%, 48%, and 32%, respectively. The implantation of energetic carbon atoms in the silicon substrate resulted in the formation of an intermixing layer acting as an adhesive layer between the film and the substrate. Fig. 2 also shows that the thickness of the intermixing layer increased with the deposition energy. This is an intrinsic characteristic of deposition processes wherein the film precursors are energetic particles. The deposition energy of 80 eV that yielded the highest sp^3 content is within the experimental deposition energy range (60–100 eV) of a-C films possessing maximum sp^3 contents [29]. The latter provides supporting evidence for the appropriateness of the present MD model for the a-C/Si system.

Fig. 3 shows the effect of deposition energy on the distribution of the hydrostatic and in-plane stresses through the thickness of a-C films for deposition energy in the range of 1–120 eV. The zero depth position corresponds to the substrate surface; thus, all depth positions mentioned below have been measured from the substrate surface. A tensile stress field exists throughout the a-C film grown under conditions of deposition energy equal to 1 eV. At higher deposition energy, however, only the near-surface region of the a-C film is under tension (surface tension effect), whereas the bulk and intermixing layers are under compression. The consequence of deposition energy on film stress can be explained by considering its effect on film densification and hybridization. Specifically, low deposition energy (1 eV) does not induce energetic atom bombardment, which is a precursor to densification and the development of a compressive stress; consequently, the film structure is dominated by sp^2 hybridization and the stress is tensile. On the other hand, higher deposition energy (≥ 20 eV) promotes densification

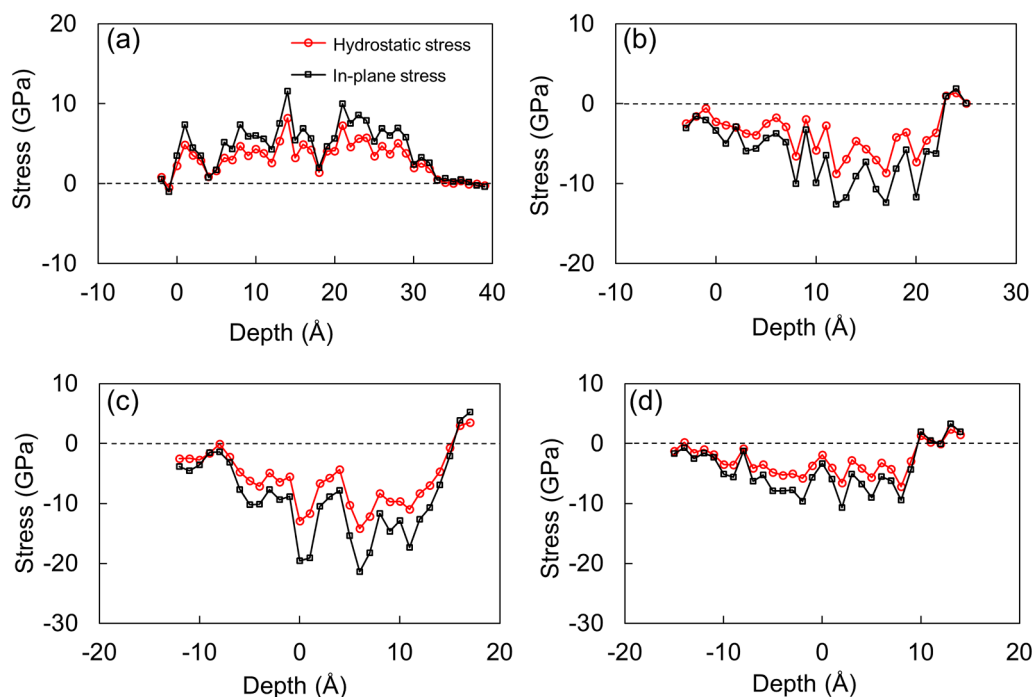


Fig. 3. Depth distributions of the hydrostatic and in-plane stresses in a-C films for carbon atom deposition energy equal to (a) 1, (b) 20, (c) 80, and (d) 120 eV. The zero depth position represents the substrate surface.

and, in turn, the development of a compressive stress state that favors sp^3 hybridization. Importantly, densification at the film surface is limited due to less pronounced energetic atom bombardment of the topmost atomic planes of the growing film. As a result, the film surface is predominantly sp^2 hybridized and the stress is tensile. Deposition energy of 80 eV produced the highest compressive stress in the film. The evolution of a dominant compressive stress field is a consequence of the bombarding effect of energetic carbon atoms. For 80 eV deposition energy, the maximum hydrostatic and in-plane stresses occur at a depth of 6 Å above the substrate surface and are equal to -14.2 and -21.3 GPa, respectively. Nevertheless, both hydrostatic and in-plane stresses decrease with the increase of deposition energy to 120 eV, showing the same trend with the sp^3 content. The internal stress predicted by the MD model is consistent with the experimental results of a previous study [30], where the internal stress of a-C films with 50% sp^3 content was found to be equal to about -16 GPa. It is known that energetic carbon atom bombardment produces a multilayered film structure consisting of intermixing, bulk, and surface layers [31]. In the present study, the boundaries of each layer were determined from the sp^3 distribution through the film thickness. Specifically, the boundaries of the intermixing and surface layers with the bulk layer existing in the middle region of the film and possessing the highest sp^3 content were identified by the instigation of a sharp decrease in the sp^3 content. The formation of Si-C bonds in the intermixing layer and the short bombardment of the structure of the surface layer are responsible for the lower sp^3 content of these layers [32]. The stress distributions for deposition energy in the range of 20–120 eV [Fig. 3(b)–(d)] demonstrate through-thickness variation similar to that of the sp^3 content, indicating the existence of a correlation between local stress and local sp^3 content.

Although the simulation results shown in Fig. 3 provide insight into the effect of deposition energy on the development of film stress, they do not reveal how the film stress and structure evolve during the film growth. An advantage of the MD analysis is that it can capture the progression of the structure and internal stress in the modeled system. Consequently, spatiotemporal distributions of the foregoing quantities were obtained from 1-Å-thick horizontal slices used to compute the average in-plane stress, sp^3 content, and number of carbon atoms at

various depths during the film growth process. Fig. 4 shows simulation results revealing changes in the in-plane stress, sp^3 content, and number of carbon atoms versus time at depth locations in the a-C film of 3, 6, and 9 Å above the substrate surface for deposition energy equal to 80 eV. Considering that the film growth simulation comprised the sequential deposition of 2000 carbon atoms, the 0.4 ns time scale in the plots of Fig. 4 is equivalent to 200 new incident carbon atoms, whereas the time range of ≥ 4 ns represents post-growth relaxation. Fig. 4(a) and (b) show similar temporal variations of the in-plane stress and sp^3 content; however, the time for the average sp^3 content at each depth position to stabilize appears to be longer than that for the average number of carbon atoms to stabilize at the same locations [Fig. 4(c)]. For instance, the average number of carbon atoms at a depth position of 3 Å stabilized after ~ 2 ns, whereas the average sp^3 content at the same location stabilized after ~ 3.2 ns. The stabilized average number of carbon atoms at a given location indicates local carbon saturation. However, the former was not conducive to high sp^3 hybridization at a specific location because the constraint provided by material from above was not adequate to effectively prevent stress relaxation because carbon atom deposition was still ongoing. This is evidenced from Fig. 4(b) and (c) showing that a maximum sp^3 content was reached at the 3 Å depth position only after the instigation of carbon atom saturation at the 6 Å depth position. Further insight into the deposition process can be obtained by considering the temporal variation of the average number of new incident carbon atoms at various depth positions [Fig. 4(d)]. From Fig. 4(b) and (d), it may be inferred that the sp^3 content at the 3 Å depth position reached a maximum after 3.2 ns when virtually no more incident carbon atoms arrived at that location. Nevertheless, the sp^3 content at the 9 Å depth position continued to increase because there were still new incident carbon atoms arriving at this location even after 4 ns. Consequently, it may be interpreted that new incident carbon atoms formed new sp^3 sites when a spatial constraint was imposed by atoms depositing above the particular location, resulting in both higher compressive stress and higher sp^3 content in deeper film regions.

As mentioned earlier, a-C films with sp^3 -rich structures are desirable protective overcoats. For this reason, the structural stability of a-C films

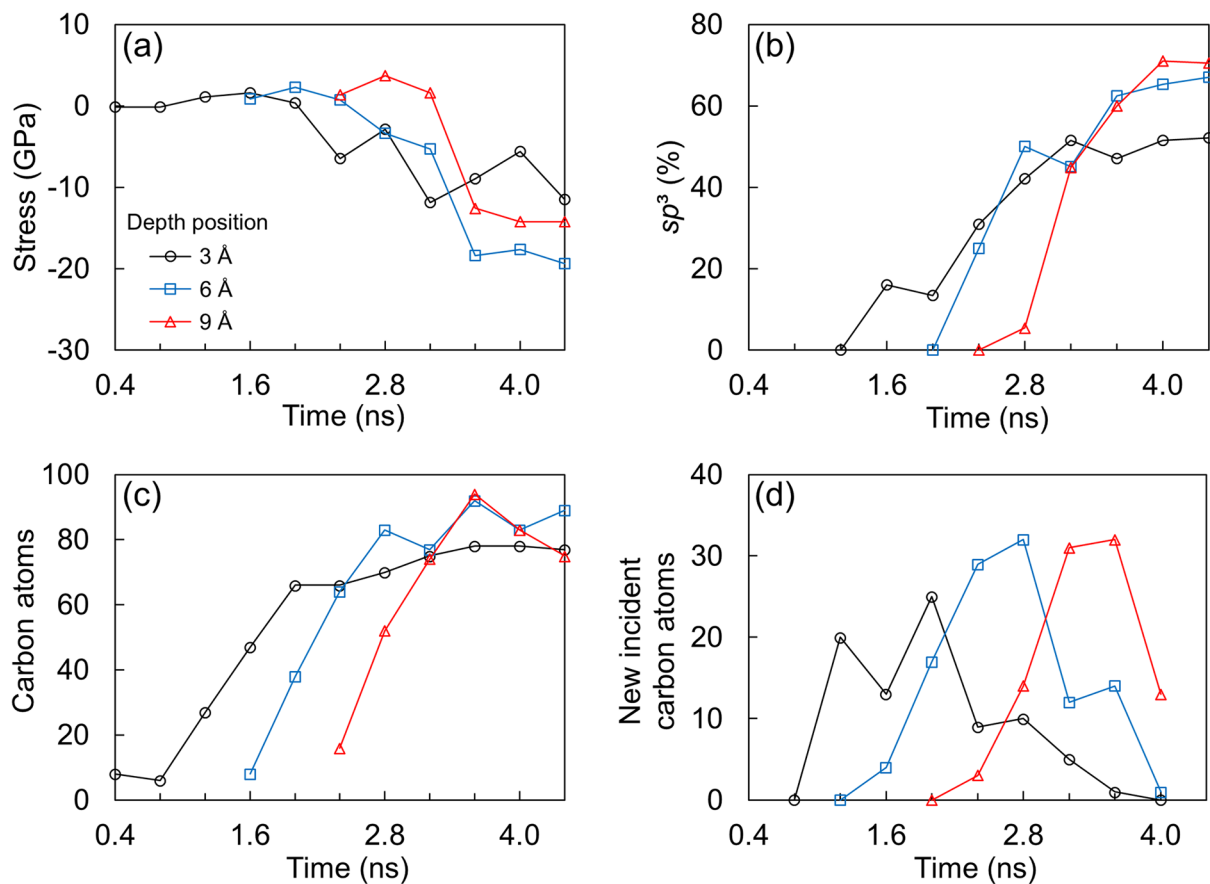


Fig. 4. Temporal variation of the average (a) in-plane stress, (b) sp^3 hybridization content, (c) number of carbon atoms, and (d) number of new incident carbon atoms at depth positions of 3, 6, and 9 Å above the substrate surface for carbon atom deposition energy equal to 80 eV.

Table 1

Average in-plane stress and sp^3 content of a-C film deposited at 80 eV obtained before and after thermal annealing in the temperature range of 150–450 °C.

Annealing temperature (°C)	Average film properties	sp^3 hybridization (%)
	In-plane stress (GPa)	
0	-14.3	48
150	-14.1	47
200	-14.6	46
250	-14.2	39
300	-12.5	37
350	-12.0	33
450	-11.8	31

in elevated-temperature environments is of high importance. Consequently, thermal annealing simulations of the a-C film with 48% sp^3 hybridization grown under conditions of deposition energy equal to 80 eV were performed to investigate thermally-induced effects on the internal compressive stress, which is a prerequisite for the formation and stability of sp^3 -hybridized domains. Table 1 shows that both the average in-plane stress and sp^3 content of the a-C film sharply decreased with the increase of temperature to 250 °C and beyond, indicating that the critical temperature that defines the thermal stability of the particular a-C film is close to 250 °C. Fig. 5 shows in-plane stress distributions through the thickness of the a-C film with 48% sp^3 hybridization (deposition energy = 80 eV) obtained before and after thermal annealing at 150 and 450 °C. The vertical dashed lines show the boundaries between the intermixing, bulk, and surface layers comprising the a-C film. It can be seen that heating resulted in stress relief, especially at 450 °C. In particular, the maximum compressive in-plane stress of -21.3 GPa at the ~6 Å depth position decreased to -18.2

and -16 GPa after heating at 150 and 450 °C, respectively. The stress relief is more pronounced in the sp^3 -rich bulk layer of the a-C film. Because the in-plane stress correlates with the hybridization state in the a-C film, with compressive and tensile stresses favoring sp^3 and sp^2 hybridization, respectively [33], the decrease of the compressive in-plane stress due to thermal annealing can be associated with the simultaneous decrease of the sp^3 content. This explains the trend of the in-plane stress and the sp^3 content with increasing temperature revealed by the data given in Table 1. The thermally-induced decreasing trend of the sp^3 content observed in the present simulations is consistent with the findings of a thermal annealing study of a-C films [34].

Further insight into the effect of thermal annealing on the evolution

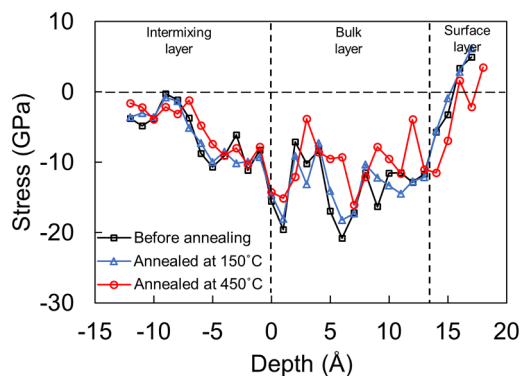


Fig. 5. Depth distribution of in-plane stress in the a-C film with 48% sp^3 hybridization content (carbon atom deposition energy = 80 eV) before and after annealing at 150 and 450 °C. The boundaries of the intermixing, bulk, and surface layers are shown by vertical dashed lines.

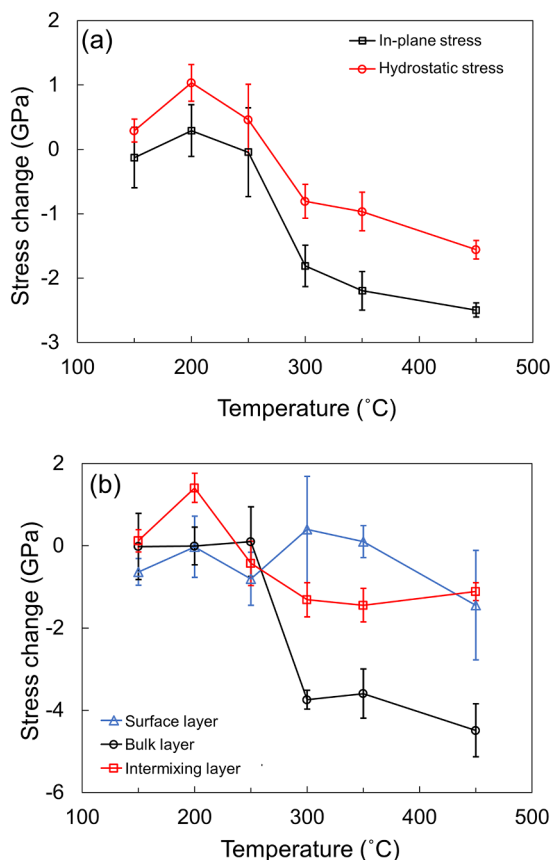


Fig. 6. Change of in-plane and hydrostatic stress in the a-C film with 48% sp³ hybridization content (carbon atom deposition energy = 80 eV) versus annealing temperature: (a) through-thickness average stress change and (b) average in-plane stress change in the surface, bulk, and intermixing layers of the a-C film. A negative stress change indicates a decrease in compressive stress.

of the film stress can be obtained in the light of the simulation results of stress change shown in Fig. 6 for the a-C film with 48% sp³ content (deposition energy = 80 eV). The change in stress averaged through the

film thickness versus annealing temperature [Fig. 6(a)] reveals the existence of a critical temperature for stress relief of ~250–300 °C, consistent with the data given in Table 1. The different critical temperature ranges of stress relief (250–300 °C) and sp³ drop (200–250 °C) are attributed to the increase of the thermal stress with annealing temperature and the simultaneous decrease of the intrinsic stress due to thermally-induced sp³→sp² rehybridization, leading to the decrease of the internal stress, which is the sum of the thermal and intrinsic stresses, in a slightly higher temperature range compared to the sp³ drop. The change of the compressive in-plane and hydrostatic stresses with increasing temperature follows a similar trend, characterized by a sharp decrease between 250 and 300 °C. In the temperature range of 300–450 °C, the change in average in-plane and hydrostatic stress is in the range of 12.7–16.8% and 9.4–16.7%, respectively. Fig. 6(b) shows the average in-plane stress change in each layer of the a-C film versus temperature. The in-plane stress in the sp²-dominated structure of the intermixing and surface layers shows very small changes due to the temperature variation compared to the sp³-rich bulk layer. Specifically, heating at 300, 350, and 450 °C caused the average in-plane stress in the bulk layer to decrease by 3.7, 3.6, and 4.5 GPa, i.e., 15.6%, 15%, and 22%, respectively. These results indicate that, although the stress changed throughout the film thickness, the stress relief was more pronounced in the bulk layer. Because a high compressive stress is a prerequisite for sp³ hybridization, as confirmed by a previous experimental study [35], it may be inferred that the decrease of the compressive in-plane stress in each layer of the a-C film correlates to the corresponding decrease in sp³ content.

As mentioned earlier, a major advantage of the MD analysis is that it can provide insight into the spatiotemporal variations of the internal stress and structure of the modelled system. Fig. 7 shows the average in-plane stress in the surface, bulk, and intermixing layers of the a-C film with 48% sp³ content (deposition energy = 80 eV) versus annealing time at various temperatures. The evolution of the in-plane stress in the three layers is consistent with the results shown in Fig. 6(b), illustrating significant stress changes in the bulk layer at 300, 350, and 450 °C. The stress relief during thermal annealing can be attributed to two simultaneously occurring processes, namely sp³→sp² rehybridization and atomic migration. Although the volume of sp² sites is larger than that of sp³ sites, the in-plane size of sp² sites is smaller due to the shorter bond length [30]. Consequently, the sp³→sp² rehybridization

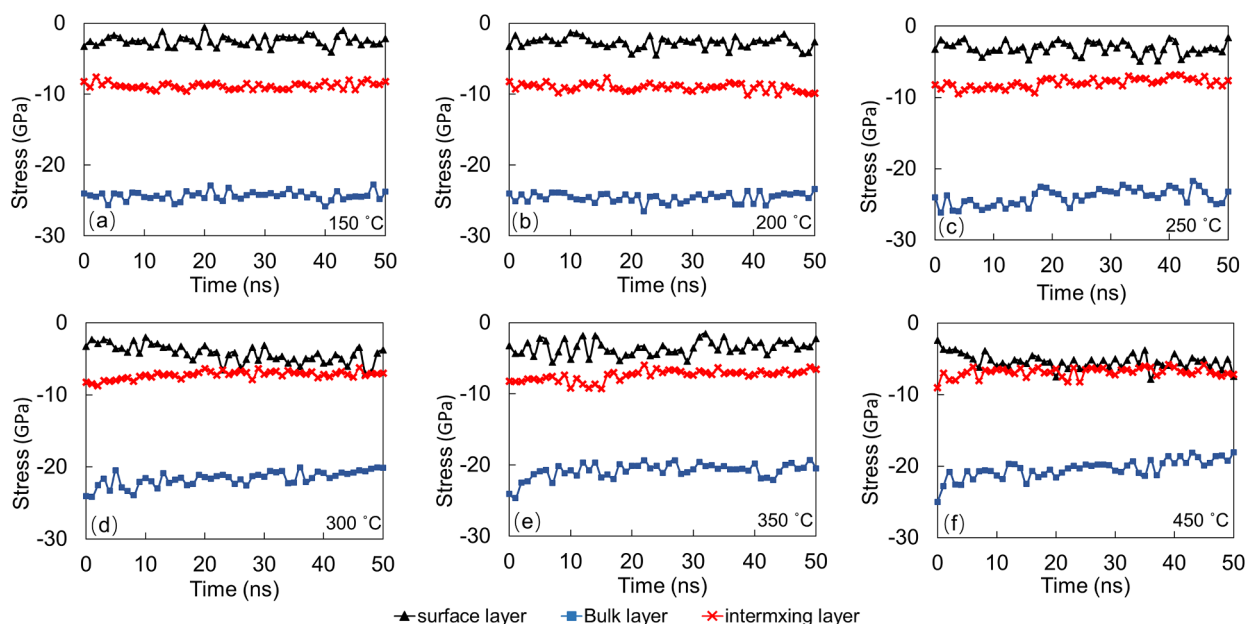


Fig. 7. Average in-plane stress in the surface, bulk, and intermixing layers of the a-C film with 48% sp³ hybridization content (carbon atom deposition energy = 80 eV) versus annealing time for temperature equal to (a) 150 °C, (b) 200 °C, (c) 250 °C, (d) 300 °C, (e) 350 °C, and (f) 450 °C.

contributes to the film stress relief from a volumetric change standpoint. The atomic rearrangement of sp^2 sites can lead to a volume decrease at the expense of a small decrease in sp^3 content [30,36]. The significant decrease of the sp^3 content after thermal annealing at a temperature of ≥ 250 °C revealed by the MD simulations of this study indicates that $sp^3 \rightarrow sp^2$ rehybridization was the major contributing factor to the stress relief in the a-C film. Nevertheless, the role of atomic rearrangement in thermally-induced stress relief needs further investigation.

The effects of the deposition energy and annealing temperature on the nanostructure and internal stress of the a-C films observed in the present analysis should be qualitatively similar for other substrate materials. Although the substrate may affect the nanostructure and properties of the intermixing layer, the effect on the bulk and surface layers of the a-C film is rather secondary in deposition methods involving energetic atom bombardment. In addition, the findings of an optimum deposition energy for sp^3 -rich a-C film growth, the existence of a critical temperature range of film stress relief, and the variation of the film stress with the annealing temperature, should also be applicable to different substrate materials, as shown by the existence of an optimal deposition energy for a-C film growth on diamond [25], for example.

It is well established that the development of a compressive stress in a-C films synthesized by deposition methods wherein the film precursors are energetic particles is a consequence of the intensive bombardment effect. An important contribution of this study is the elucidation of the underlying factors affecting the evolution of compressive stress in ultrathin a-C films, the correlation of film stress with sp^3 hybridization, the dependence of the former on local carbon atom saturation, and the stress relief above a critical temperature. The latter reveals the existence of an energy barrier that stabilizes the compressive stress in the a-C film, primarily in the sp^3 -dominant bulk layer. Consequently, thermal annealing provides the energy needed to overcome the energy barrier for relaxing the compressive stress generated in the film during the deposition process [36].

4. Conclusions

The origins of internal stress in ultrathin a-C films synthesized by energetic particle bombardment processes and the effect of thermal annealing on stress relief were examined in the light of MD simulation results. It was shown that the high compressive stress generated in the films correlates with the amount of sp^3 hybridized atomic carbon, especially in the sp^3 -rich bulk layer of the multilayered a-C film structure. Importantly, a high compressive stress, which is a precondition for high sp^3 hybridization, emerges at a film location only when the incident carbon atoms at that location have been spatially constrained by the carbon-saturated atomic plane from above. For a-C films with 48% sp^3 hybridization, a significant stress relief was encountered after thermal annealing at a temperature of ≥ 250 °C. Simulations confirmed that the stress relief mainly commenced in the bulk layer of the a-C film and that the internal stress of the annealed a-C film decreased rapidly, suggesting that film stress relaxation is a very fast process. The two main mechanisms responsible for the stress relief during thermal annealing were found to be $sp^3 \rightarrow sp^2$ rehybridization and atomic migration. The results of this MD study provide insight into the spatio-temporal evolution of internal stress in ultrathin a-C films and the underlying physics that correlate the distribution and magnitude of internal stress with structural changes activated by thermal annealing.

Author statement

S.W. performed all the MD simulations and wrote the first draft of the paper. K.K. defined the scope of the entire work, supervised the research of S.W., examined the simulation results, and wrote the final manuscript of the paper.

Declaration of Competing Interest

The authors declare that they have no known competing financial interests or personal relationships that could have appeared to influence the work reported in this paper.

Acknowledgments

This research was funded by Western Digital Technologies, Inc. The authors acknowledge the use of the Savio computational cluster resource provided by the Berkeley Research Computing program at the University of California, Berkeley.

References

- [1] Y. Taki, O. Takai, XPS structural characterization of hydrogenated amorphous carbon thin films prepared by shielded arc ion plating, *Thin Solid Films* 316 (1998) 45–50.
- [2] Q. Zhang, S.F. Yoon, Rusli, J. Ahn, H. Yang, D. Bahr, Deposition of hydrogenated diamond-like carbon films under the impact of energetic hydrocarbon ions, *J. Appl. Phys.* 84 (1998) 5538–5542.
- [3] M. Weiler, S. Sattel, K. Jung, H. Ehrhardt, V.S. Veerasamy, J. Robertson, Highly tetrahedral, diamond-like amorphous hydrogenated carbon prepared from a plasma beam source, *Appl. Phys. Lett.* 64 (1994) 2797–2799.
- [4] J. Xie, K. Komvopoulos, Hybridization and tribomechanical properties of ultrathin amorphous carbon films synthesized by radio-frequency low-pressure plasma discharges, *Surf. Coat. Technol.* 262 (2015) 15–20.
- [5] J. Matlak, K. Komvopoulos, Friction properties of amorphous carbon ultrathin films deposited by filtered cathodic vacuum arc and radio-frequency sputtering, *Thin Solid Films* 579 (2015) 167–173.
- [6] G.W. Malaczynski, A.H. Hamdi, A.A. Elmoursi, X. Qiu, Diamond-like carbon coating for aluminum 390 alloy – automotive applications, *Surf. Coat. Technol.* 93 (1997) 280–286.
- [7] A.A. Voevodin, J.P. O'Neill, J.S. Zabinski, Nanocomposite tribological coatings for aerospace applications, *Surf. Coat. Technol.* 116–119 (1999) 36–45.
- [8] L.A. Thomson, F.C. Law, N. Rushton, J. Franks, Biocompatibility of diamond-like carbon coating, *Biomaterials* 12 (1991) 37–40.
- [9] P.R. Goglia, J. Berkowitz, J. Hoehn, A. Xidis, L. Stover, Diamond-like carbon applications in high density hard disc recording heads, *Diamond Relat. Mater.* 10 (2001) 271–277.
- [10] P. Wang, X. Wang, T. Xu, W. Liu, J. Zhang, Comparing internal stress in diamond-like carbon films with different structure, *Thin Solid Films* 515 (2007) 6899–6903.
- [11] J.P. Sullivan, T.A. Friedmann, K. Hjort, Diamond and amorphous carbon MEMS, *MRS Bull.* 26 (2001) 309–311.
- [12] J. Robertson, Deposition mechanisms for promoting sp^3 bonding in diamond-like carbon, *Diamond Relat. Mater.* 2 (1993) 984–989.
- [13] J. Robertson, The deposition mechanism of diamond-like a-C and a-C:H, *Diamond Relat. Mater.* 3 (1994) 361–368.
- [14] H. Windischmann, G.F. Epps, Y. Cong, R.W. Collins, Intrinsic stress in diamond films prepared by microwave plasma CVD, *J. Appl. Phys.* 69 (1991) 2231–2237.
- [15] E. Liu, L. Li, B. Blanpain, J.P. Celis, Residual stresses of diamond and diamondlike carbon films, *J. Appl. Phys.* 98 (2005) 073515.
- [16] N. Dwivedi, S. Kumar, H.K. Malik, Superhard behaviour, low residual stress, and unique structure in diamond-like carbon films by simple bilayer approach, *J. Appl. Phys.* 112 (2012) 023518.
- [17] B.K. Tay, X. Shi, E.J. Liu, H.S. Tan, L.K. Cheah, Effects of substrate temperature on the properties of tetrahedral amorphous carbon films, *Thin Solid Films* 346 (1999) 155–161.
- [18] W. Dai, X. Gao, J. Liu, Q. Wang, Microstructure, mechanical property and thermal stability of diamond-like carbon coatings with Al, Cr and Si multi-doping, *Diamond Relat. Mater.* 70 (2016) 98–104.
- [19] B.K. Tay, X. Shi, E. Liu, S.P. Lau, L.K. Cheah, Z. Sun, J. Shi, Stress relief of tetrahedral amorphous carbon films by post-deposition thermal annealing, *Surf. Coat. Technol.* 120–121 (1999) 448–452.
- [20] J. Belak, I.F. Stowers, Molecular dynamics studies of surface indentation in two dimensions, *Mater. Res. Soc. Symp. Proc.* 193 (1990) 259–264.
- [21] J. Belak, I.F. Stowers, The indentation and scraping of a metal surface: a molecular dynamics study, in: Singer, I.L., Pollock, H.M. (eds.), *Fundamentals of Friction: Macroscopic and Microscopic Processes*, NATO ASI Series (Series E: Applied Sciences), Springer, Dordrecht, 1992, vol. 220, pp. 511–520.
- [22] W. Yan, K. Komvopoulos, Three-dimensional molecular dynamics analysis of atomic-scale indentation, *ASME J. Tribol.* 120 (1998) 385–392.
- [23] J. Yang, K. Komvopoulos, A molecular dynamics analysis of surface interference and tip shape and size effects on atomic-scale friction, *ASME J. Tribol.* 127 (2005) 513–521.
- [24] J. Yang, K. Komvopoulos, A stress analysis method for molecular dynamics systems, *Int. J. Solids Struct.* 193–194 (2020) 98–105.
- [25] T. Ma, Y.-Z. Hu, H. Wang, X. Li, Microstructural and stress properties of ultrathin diamondlike carbon films during growth: molecular dynamics simulations, *Phys. Rev. B* 75 (2007) 035425.
- [26] J. Tersoff, Modeling solid-state chemistry: interatomic potentials for

- multicomponent systems, *Phys. Rev. B* 39 (1989) 5566–5568.
- [27] J. Tersoff, Erratum: Modeling solid-state chemistry: interatomic potentials for multicomponent systems, *Phys. Rev. B* 41 (1990) 3248.
- [28] V. Vitek, T. Egami, Atomic level stresses in solids and liquids, *Phys. Status Solidi (b)* 144 (1987) 145–156.
- [29] J. Robertson, Diamond-like amorphous carbon, *Mater. Sci. Eng. R: Rep.* 37 (2002) 129–281.
- [30] A. Ferrari, S. Rodil, J. Robertson, W. Milne, Is stress necessary to stabilise sp^3 bonding in diamond-like carbon? *Diamond Relat. Mater.* 11 (2002) 994–999.
- [31] N. Wang, K. Komvopoulos, The multilayered structure of ultrathin amorphous carbon films synthesized by filtered cathodic vacuum arc deposition, *J. Mater. Res.* 28 (2013) 2124–2131.
- [32] C.A. Davis, G.A.J. Amaratunga, K.M. Knowles, Growth mechanism and cross-sectional structure of tetrahedral amorphous carbon thin films, *Phys. Rev. Lett.* 80 (1998) 3280–3283.
- [33] W. Lu, K. Komvopoulos, Effect of stress-induced phase transformation on nanomechanical properties of sputtered amorphous carbon films, *Appl. Phys. Lett.* 82 (2003) 2437–2439.
- [34] J. Matlak, E. Rismaniyazdi, K. Komvopoulos, Nanostructure, structural stability, and diffusion characteristics of layered coatings for heat-assisted magnetic recording head media, *Sci. Rep.* 8 (2018) 9807.
- [35] J. Xie, K. Komvopoulos, Thermal stability of ultrathin amorphous carbon films synthesized by plasma-enhanced chemical vapor deposition and filtered cathodic vacuum arc, *Philo. Mag.* 97 (2017) 820–832.
- [36] P.C. Kelires, Intrinsic stress and local rigidity in tetrahedral amorphous carbon, *Phys. Rev. B* 62 (2000) 15686–15694.